

## Numerical-experimental study on the thickness distribution of metallic bipolar plates for PEM fuel cells

Hossein Talebi-Ghadikolaee<sup>1</sup>, Mohammad Mahdi Barzegari<sup>2,\*</sup>, Farzad Ahmadi Khatir<sup>3</sup>, Shahaboddin Seddighi<sup>3</sup>

<sup>1</sup> Faculty of Mechanical Engineering, University of Kashan, Kashan, Iran

<sup>2</sup> Northern Research Center for Science and Technology, Malek Ashtar University of Technology, Iran

<sup>3</sup> Faculty of Mechanical Engineering, Tarbiat Modares University, Iran

### Article Information

Article History:

Received:

22 Sep 2021

Received in revised form:

01 Dec 2021

Accepted:

08 Dec 2021

### Keywords

Polymer electrolyte membrane fuel cell

Metallic bipolar plate

Metal forming

Thickness distribution

Strain path

### Abstract

In this study, the plastic deformation of a metallic bipolar plate with a serpentine flow field was investigated during the stamping process. The strain path and thickness distribution in 304 stainless steel bipolar plates with a thickness of 0.1 mm were determined. To achieve this purpose, the process was simulated by the ABAQUS commercial finite element code, and the validity of the results was evaluated by experimental tests under simple and lubricated conditions. According to the results, the flow of material has a significant effect on the thickness distribution of the central and lateral channels, and the thickness reduction percentage of the central channel in the longitudinal, diagonal, and transverse directions is higher than the lateral one. The maximum thickness reduction in the central channels is observed in the longitudinal direction, while the diagonal direction is considered as a critical direction for lateral channels. Due to the existence of the equibiaxial tension strain path in the diagonal direction, significant thickness reduction is observed in both the side and the rib zone of the channels. However, using lubricant led to a decrease in the thickness reduction percentage by improving the flow of material into the die cavity. Moreover, under lubricated conditions, the critical area is transferred from the side area of the channel in the longitudinal direction to the rib area in the diagonal direction.

## 1. Introduction

Clean and renewable energy sources, such as fuel cells, are one of the main alternatives to fossil fuels in

various industries. Fuel cells are widely used in the transportation industry because of their higher efficiency and lower pollution compared to internal combustion engines [1, 2]. Among the types of fuel

\*Corresponding Author: Barzegari@mut.ac.ir

cells, polymer electrolyte membrane (PEM) fuel cell has received more attention due to their higher efficiency, higher current density, and lower operating temperature [3].

Polymer electrolyte membrane fuel cells (PEMFCs) are composed of various components, including a gas diffusion layer (GDL), catalyst layer, bipolar plates (BPPs), and end plates [4]. Bipolar plates (BPPs) make up a significant percentage of the weight and marginal cost of PEMFCs [5] and are materially divided into three groups of graphite [6], composite [7], and metallic [8] plates. Due to their desirable mechanical properties and high electrical conductivity, metallic bipolar plates (MBPPs) have received more attention than many other types of BPPs [9]. Aluminum [10], titanium [11], and stainless steel alloys [12] are used to produce these plates. To control the fuel flow and the output of the reactions on the catalyst layers, MBPPs have flow paths with various patterns such as pin-type, parallel, serpentine, parallel-serpentine, radial, etc. [13]. Accordingly, machining and metal forming processes are employed to produce MBPPs [9, 14]. Among these methods, metal forming has received much attention due to the simplicity of the process, reduced production cost, high production speed, and appropriate surface quality.

Several studies have been performed to determine the effect of process parameters to increase the quality of MBPPs. Yang et al. [15] produced MBPPs using the additive manufacturing method. According to their results, the produced plate performs well in a PEMFC, and a current density of  $2 \text{ A/m}^3$  at  $1.779 \text{ V}$  can be achieved. Mohammadtabar et al. [16] studied the fabrication of MBPPs using the hydroforming process. They found that increasing the forming pressure increases the mold filling (increasing the stretch ratio) as well as the thinning percentage. Elyasi et al. [17] investigated the rubber shape of MBPPs with a spiral grooving pattern. They proposed a novel way to enhance the quality of MBPPs

by modifying the shape of the rubber layer in the rubber forming process. Talebi-Ghadikolaei et al. [18] studied the fracture defect in the rubber pad forming of parallel micro-channels of MBPPs. They employed three fracture criteria to predict the fracture of sheets. Abeyrathna et al. [19] used a roll forming process to produce MBPPs. The essential conditions were applied to increase the channel depth and decrease the thinning due to lower sheet elasticity compared to hydroforming and rubber forming processes.

The stamping process has also received special attention as one of the suitable processes for the fabrication of BPPs due to the simplicity of the process, high production speed, and lower production costs [20]. Hu et al. [21] investigated the MBPP stamping process experimentally and by theoretical simulations. They examined the influence of process parameters and used the forming limit curve to determine the safe area. To increase channel depth and minimize thinning percentages, Bong et al. [22] investigated the multi-stage stamping process of MBPPs. Choi et al. [23] and Jin et al. [24] used the effect of heat treatment processes and dynamic loading conditions to improve the quality of the MBPPs. Neto et al. [25] used finite element analysis to simulate two separate zones in longitudinal (straight) and diagonal (U-bend) directions of the flow field to investigate the stamping process of the MBPPs. According to their results, the U-bend channel section is the most critical zone in terms of thinning.

Thus far, valuable studies have been carried out on the various processes used to fabricate MBPPs. The influence of process parameters on channel depth and thickness distribution has also been investigated. However, the effect of the number of channels and variation of material flow during plastic deformation on the quality of the various location of the MBPP fabricated by the stamping process has not been investigated. This issue is important because of the existence of various deformation mechanics in different areas of the MBPP with a serpentine

flow field. Since the complex patterns of the micro-channels and different zone of each channel of MBPPs are related to each other, the deformation mechanics of the different zones of micro-channels are no longer uniform. These variations of deformation mechanics along with various directions and their effect on the fabricated sample (thinning and critical area) should be investigated comprehensively. This issue has not been considered in previous studies. These issues become more important in dead-ended PEMFCs in which the micro-channels with a high channel depth and a low ratio of the channel width to depth are required.

In the present study, the stamping process of a 304 stainless steel (SS304) bipolar plate with a parallel-serpentine pattern was investigated. Due to the variation of deformation mechanics at different locations of MBPPs with serpentine flow fields, this study aimed to explore the effect of the number of micro-channels on the trend of thickness distribution in different directions. The strain path in critical areas and its effect on the thickness distribution were determined. Finally, the effect of modified process conditions (lubrication) on the sheet flow was studied, and the direction and critical areas under different forming conditions were determined. The novelty of this work is twofold: (i) Accurate modeling of the forming conditions considering the interaction effect of various zones along the longitudinal, diagonal, and transverse direction of the serpentine micro-channels of dead-ended PEMFCs regarding the investigation of the sheet metal flow, deformation mechanics (strain path) during the stamping process, thickness distribution, and the position of the critical area of the MBPPs. (ii) Modifying the stamping process using the effect of lubrication on the location of critical areas and the directional thickness distribution of MBPPs.

## 2. Laboratory procedures

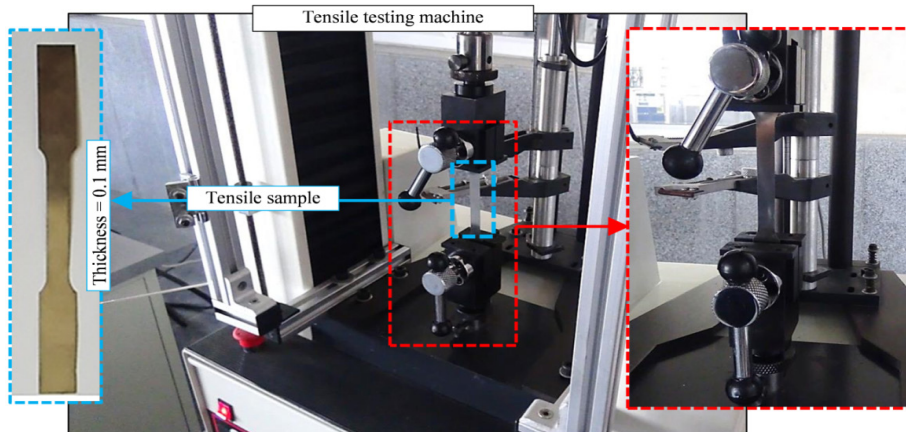
### 2.1. Mechanical properties of SS304

The plasticity behavior of the stainless steel 304 (SS304) sheet was identified using uniaxial tensile tests. As shown in Fig. 1(a), samples were prepared in dimensions per ASTM E8 using wire cutting. It is worth noting that an ultra-thin SS304 annealed sheet with a thickness of 0.1 mm in which the anisotropic behavior is not impressive was used as a primary blank. Therefore, the anisotropy of the sheet was ignored.

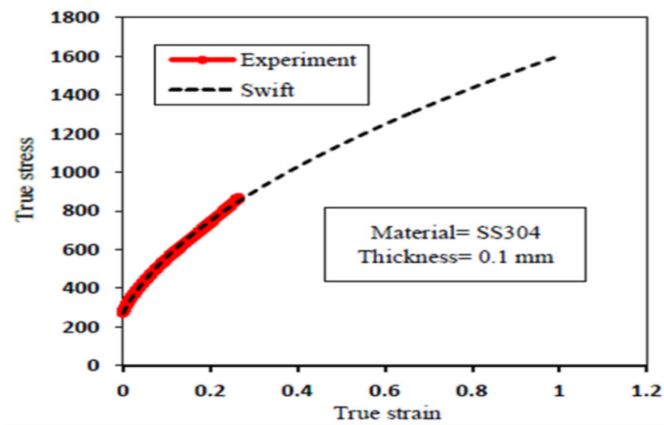
The hardening rule is another critical part of the plasticity model. The Swift law was adopted to obtain a reliable stress-strain relationship beyond necking as follows:

$$\bar{\sigma} = A (\varepsilon_0 + \varepsilon_p)^n \quad (1)$$

where  $A$ ,  $\varepsilon_0$ ,  $n$ , and  $\bar{\varepsilon}_p$  denote the strength coefficient, the pre-strain, the hardening exponent, and plastic strain, respectively. The hardening rule constants were determined using the experimental true stress-strain curve (inverse method). The experimentally measured true-stress strain curve and calibrated Swift law results are shown in Fig. 1(b). The obtained material properties are summarized in Table 1.



(a)



(b)

Fig. 1. (a) Uniaxial tensile test sample and the tensile testing machine and (b) true stress-strain curve and calibrated swift law results.

Table 1. Mechanical properties along the rolling direction together with the Lankford coefficients.

Material Data	
Density (kg/m <sup>3</sup> )	7800
Young's modulus (GPa)	200
Yield strength (MPa)	271
Hardening law of the material	
$A$ (MPa)	1576
$n$	0.51
$\epsilon_0$	0.0315

## 2.2. Forming MBPPs

In this study, the stamping process was used to form a 0.1 mm-thick steel sheet and to produce the SS304

MBPPs. The MBPP stamping die consisted of the punch and the matrix on which MBPP micro-channels were machined. Micro-channels with rib and channel widths of 1.1 and 0.5 mm, respectively, were investigated in this study. The inner radius ( $r$ ) and outer corner radius ( $R$ ) were equal to 0.3 and 0.2 mm, respectively, and the draft angles were equal to 10°. The dimensions of the machined channels on the punch and die surface were designed to fit the final plate dimensions. A 60-ton press was used for loading. The die, press, and dimensions of the micro-channels are shown in Fig. 2.

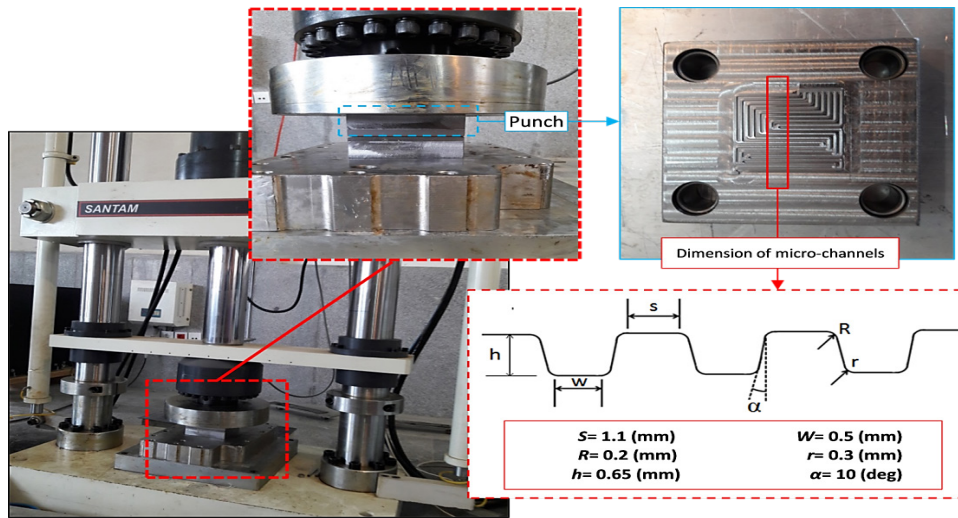


Fig. 2. Dimension of the metallic bipolar plates' micro channel together with the experimental equipment.

To investigate the thickness distribution and profile of the formed specimens, MBPPs were cut after the forming operation using a wire cutting machine in longitudinal, transversal, and diagonal directions. Fig. 3 illustrates the phases of specimen preparation and

the optical microscope image of the cross-section of the fabricated MBPP. It should be mentioned that all the experiments were repeated three times, and the average value of the intended outputs are reported in the following section.

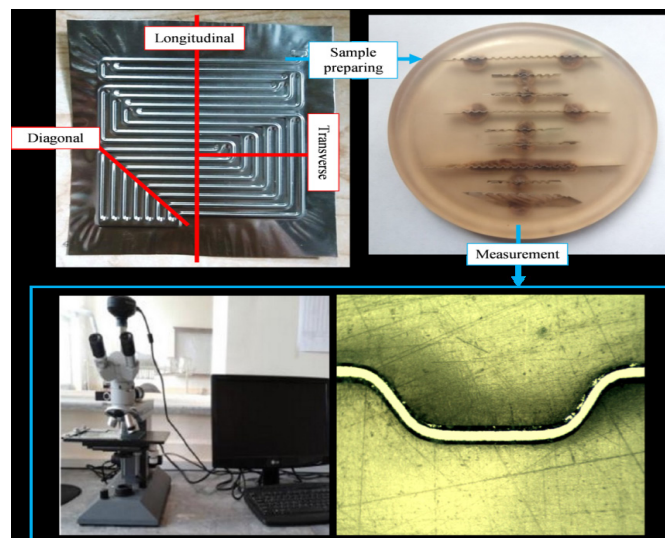


Fig. 3. The measuring process of the stamped MBPPs.

### 3. Finite Element Simulation

The ABAQUS finite element commercial code was used to simulate the process. The process was modeled without considering the symmetry. Punch and die

were rigidly modeled. Since the thickness of the blank during stamping is significantly smaller than the other two dimensions, the process was assumed as plane stress, and the sheet metal was modeled shell-like and deformable. The R3D4 and S4R elements with dimen-

sions of 0.065 and 0.1 mm were used for discretizing the geometry of the sheet and mold, respectively. The mechanical properties of the sheet were applied in the simulation according to Table 1. The calibrated Swift law (Sec. 2) was employed to define the strain hardening of the sheet metal. Moreover, the plastic behavior of the sheet metal was assumed to be isotropic and modeled by the von Mises yield function. To apply force on the sheet metal, the displacement boundary condition was applied to the punch while the die was bound in all directions, and no boundary conditions were applied to the sheet metal. Surface-to-surface contact conditions between the punch, the die, and

the sheet were defined with a friction coefficient of 0.2 under non-lubricated conditions and 0.1 under lubricated conditions. The friction coefficients were determined using iterative simulation and compared experimentally and numerically. A comparison of the experimentally measured and numerically predicted thickness distributions indicates that the numerical model is capable of providing a close description of the experiments when the friction coefficients were considered equal to 0.2 and 0.1 for non-lubricated and lubricated conditions, respectively. The finite element model is shown in Fig. 4.

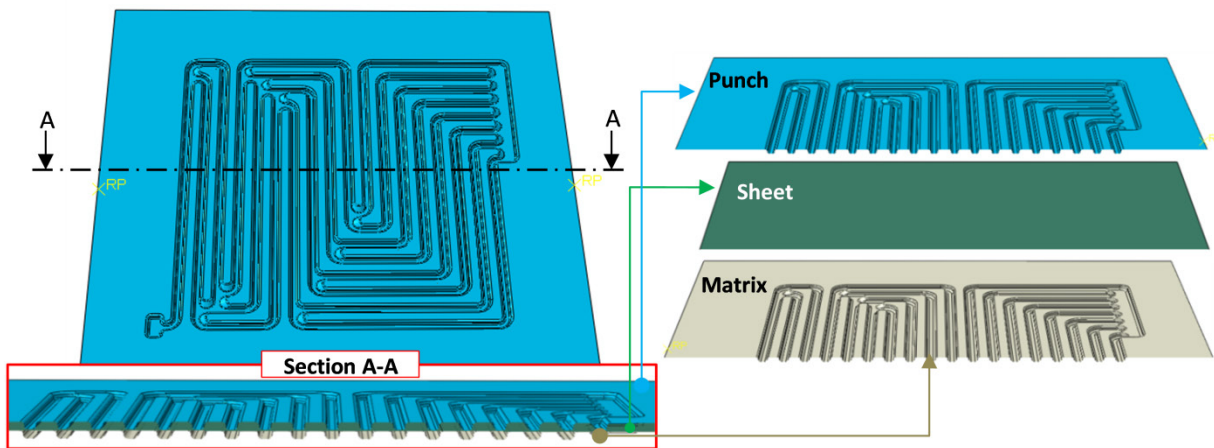


Fig. 4. Finite element model of the stamping process.

## 4. Results and discussion

The force-displacement and thickness distribution curves obtained from experimental tests and numerical investigations were evaluated to validate the accuracy of the simulation results in predicting the plastic behavior (Fig. 5). According to the results, a good agreement was observed between the experimentally measured and numerically predicted results. This confirms the accuracy of the results of finite element modeling to determine the plastic behavior and con-

tact properties in the MBPP stamping process. Hence, the proposed model was used to define the thickness distribution and strain path during the fabrication of MBPPs. It is worth noting that the channel depth to width ratio of the micro-channel is one of the most important factors in the efficiency of the PEM fuel cell. On the other hand, substantial thickness reduction during stamping of thin metallic bipolar plates is the crucial limiting factor for obtaining the appropriate value of channel depth. Though promising results have been shown in previous studies related to the forming

of metallic bipolar plates, researchers were focused on the effect of single-channel parameters on the increasing or decreasing trends of thickness reduction and filling percentage [10, 16, 20, 26]. It is noticeable that separate modeling of various areas could not accurately represent the forming conditions of the stamping process of a metallic bipolar plate with a serpentine flow field because the straight channels are connected using a U-turn channel, and the plastic deformation in

different areas are related and have an effect on each other. On the other hand, the present study focused on the industrial scale of MBPPs with serpentine flow fields. A 3D finite element model was employed to fully simulate the forming process of the serpentine flow field to consider the interaction effect of micro-channels on thinning percentage results along the various directions of the serpentine flow field. The detailed results are presented in the following.

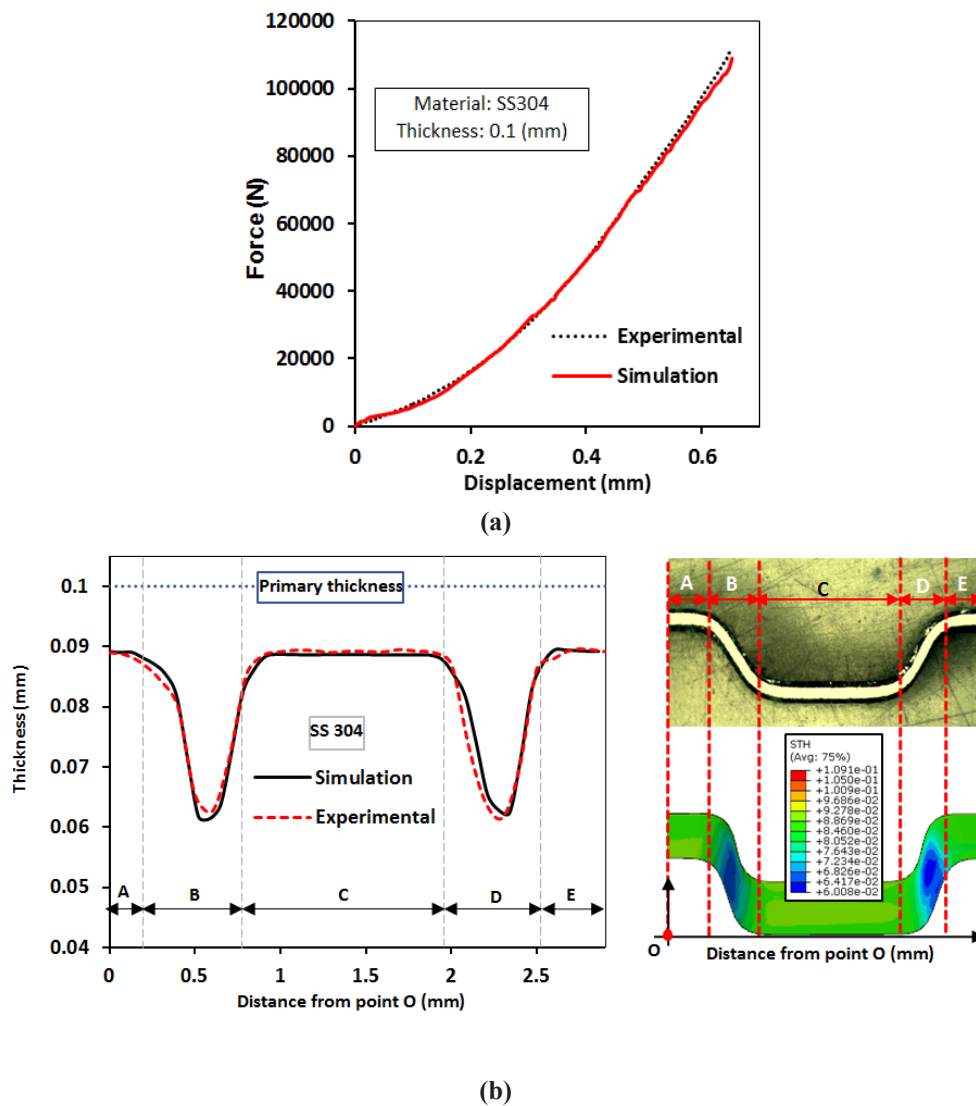


Fig. 5. (a) Finite element modeling of the forming process. (b) Comparison of experimentally measured and numerically predicted thickness distribution in SS304 MBPP.

#### 4.1. Effect of force on channel depth and thickness distribution

In this section, the accuracy of the results of the finite element modeling, the rate of deformation, and the mode of sheet flow at different stages of the process are investigated. For this purpose, the filling percentage and thickness distribution were determined when the applied forces were 40, 70, and 100 kN. Next, the ratio of the BPP channel depth to the mold channel depth (0.65 mm) was used to determine the filling percentage. The channel depth and filling percentage were raised by increasing the force. According to the results, the filling rate increased from 55.84% at 40 kN to 96.61% at 100 kN. Fig. 6(a) shows the trend of change in the percentage of filling per change in force.

Also, the thickness distribution results are shown in Fig. 6(b). As can be seen from the results, increasing both the force and channel depth decreased the thickness of the sheet in different regions. Initially, the highest decrease in thickness occurred in areas *a* and *c*. Subsequently, due to the contact between the sheet and the mold in the areas above, the sheet flow in these areas is restricted and transferred to the side area of the channel (SAC). Accordingly, during the process, the largest decrease in thickness occurred in area *b* (SAC). Due to the stamping die clearance, the part of the blank located in this area (*b*) has more freedom. Moreover, due to having less restriction, the sheet flow is concentrated in this area, which ultimately results in the greatest reduction in the thickness of the SAC (critical area).

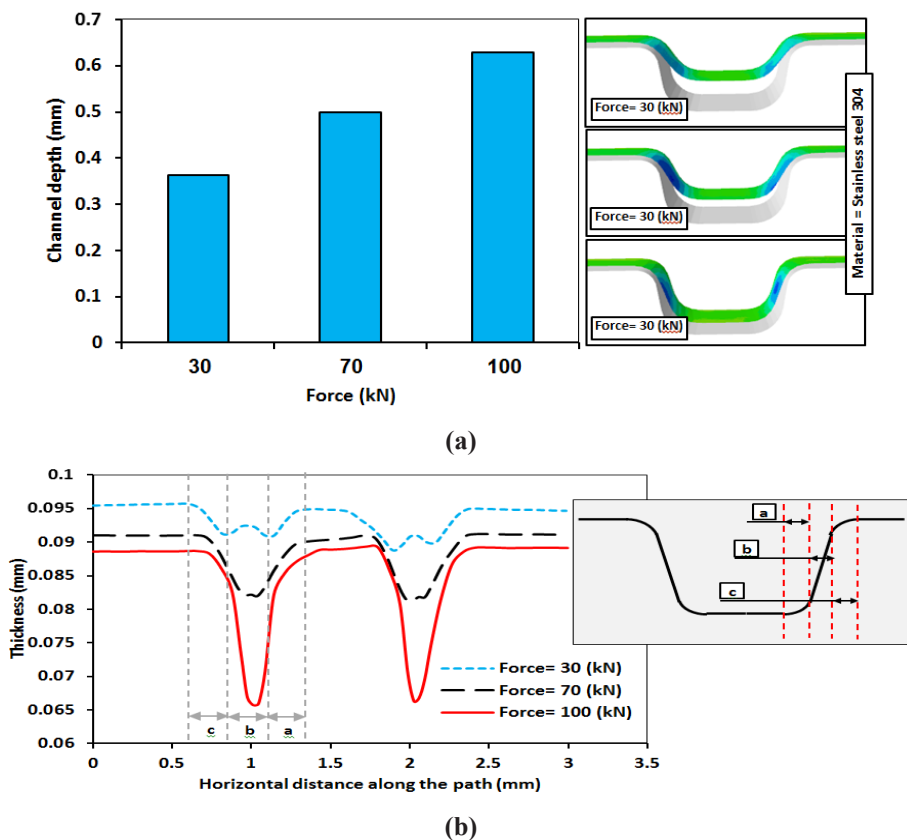


Fig. 6. Effect of force on (a) channel depth and (b) thickness distribution.

According to the thickness in the critical area, the thinning percentage was calculated based on the initial sheet thickness (0.1 mm) and the sheet thickness after deformation (according to Equation 2).

$$t_r = \left( \frac{t_0 - t_f}{t_0} \right) \times 100 \quad (2)$$

where  $t_r$ ,  $t_0$ , and  $t_f$  are the thinning percentage, initial thickness, and final thickness, respectively. According to the results, increasing the force from 40 kN to 70 and 100 kN increased the thinning percentage from 11.3% to 18.7% and 34.3%, respectively.

#### 4.2. Thickness variation in different directions of MBPP

It is important to determine the metal flow in different regions (lateral and middle regions) in this research to thoroughly investigate the MBPP formed with a serpentine flow field pattern. For this purpose, the thickness distribution in different channels along the longitudinal, transversal, and diagonal directions was studied. The position of the investigated channels is shown in Fig. 7.

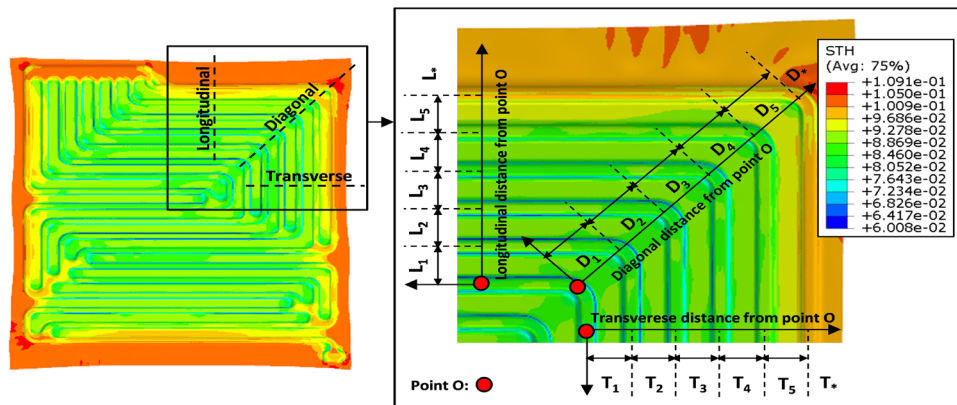


Fig. 7. Longitudinal, diagonal, and transverse direction together with the divided area.

The thickness distribution trend in the longitudinal direction L1 to L5 along L\* is shown in Fig. 8(a). According to the results obtained in all ranges, the minimum thickness was created in the SAC. Interestingly, the thickness of the specimen increased by moving toward the lateral channel (transition from L5 to L1). This is due to the flow of the blank from areas outside the micro-channels to the lateral channels, which results in a more uniform thickness distribution by feeding the sheet from non-critical areas toward the SAC. Also, according to the results, this effect is only visible in the three lateral channels (L5 to L3), and then the thinning percentage converges to a certain amount. Moreover, thickness

variations in different areas of the channel were not affected by the sheet metal flow from the lateral areas. As a result, the minimum thicknesses were almost the same in L2 and L1.

The thickness variations in different channels in the diagonal direction are shown in Fig. 8(b). Similar to the longitudinal direction, the thickness reduction in the lateral channels (D5) was also less than the middle channels (D1). Under these conditions, the sheet metal flow from the non-critical areas (D\*) toward the lateral channels also improved the thickness distribution. The effect of sheet flow from the outer regions on the thickness distribution in the diagonal direction only affected the three initial

channels (D5 to D3), and in the subsequent channels, both the maximum thinning percentage and thickness changes were the same. Furthermore, the thickness distribution non-uniformity in each channel was greater in the diagonal direction than in the longitudinal direction.

For a closer look, the process of thickness distribution changes in region D2 (Fig. 8(b)) was studied in detail. For this purpose, different points in region D2 were

selected. The selection of points was made in such a way that an appropriate dispersion was created in the different areas of the channel. The above points and the thickness distribution chart corresponding to region D2 are shown in Fig. 9. According to the results, the thickness decreased from 0.083 mm at point *a* to 0.66 mm at point *b* on the SAC (in the inner corner radius area of the spiral).

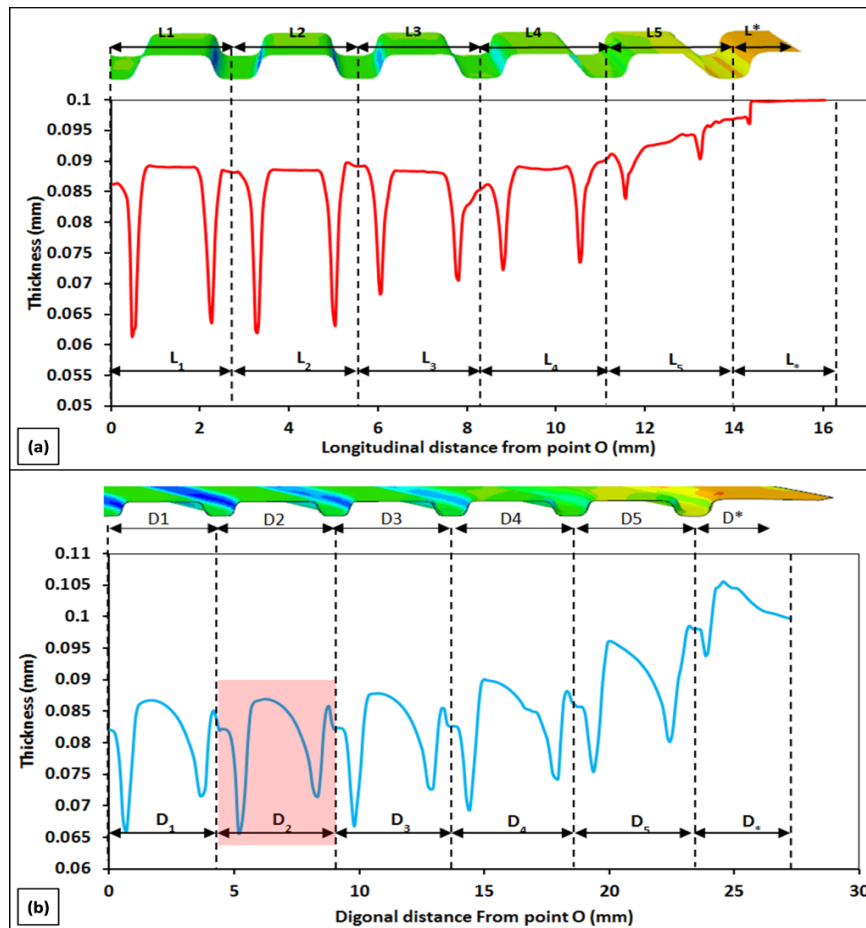


Fig. 8. Thickness distribution, (a) longitudinal direction and (b) diagonal direction.

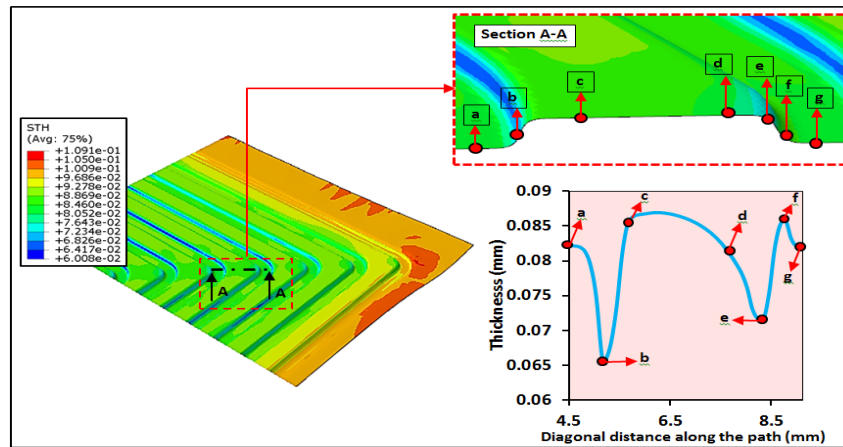


Fig. 9. Various locations in the diagonal direction and related thickness value.

The significant decrease in thickness in this area is due to the presence of the clearance between the punch and the die and more elongation of the sheet metal in this area in comparison with other areas (from contact with the punch and die surface). Points *c* and *d* are in the area where the sheet is in contact with the die surface. The frictional force between the sheet and the die reduces the sheet flow from these areas to other areas. As a result, the thickness reduction in this area was less than in other areas in the diagonal direction. In addition, the thickness of the specimen decreased with the displacement from point *c* to *d*, according to the results. This may be due to the strain path changes from the plate strain to the biaxial stretching. To investigate this, the strain path of the elements at

points *c* and *d* in the diagonal direction together with the critical element in the longitudinal direction was extracted. As shown in Fig. 10, the strain path of the longitudinal direction was exactly located at the plane strain condition with a higher plastic equivalent strain than *c* and *d*, as expected (higher thickness reduction). According to the results, the strain path at point *c* was close to the plate strain state. As it can be seen, the strain path changed to the biaxial stretching mode ( $\beta = 1$ ) when moving from point *c* to *d*. Due to the similarity of the main strain at both points, changing the state from plane strain to the biaxial stretching increased the equivalent strain and decreased the thickness at point *d* compared to point *c*.

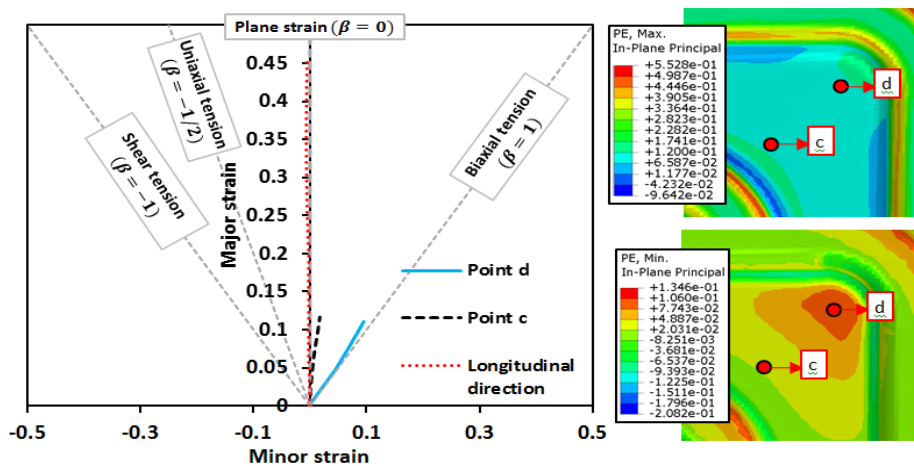


Fig. 10. Strain path in the diagonal direction.

Finally, the thickness distribution in the transversal channels in SS304 MBPPs formed by the stamping (punch and die) process was investigated. The thickness distribution in regions T1 to T5 (Fig. 7) was derived from the FES results and is shown in Fig. 11. In this case, similar to the other directions, the thickness of the sheet (after being formed) was greater in the lateral channels than in the middle channels. Since the sheet metal was fed from the lateral areas, the thick-

ness reduction in region T5 was not significant. However, the minimum thickness created in the workpiece decreased by moving toward region T1. In all areas (T1 to T5), the greatest decrease in thickness occurred in the SAC. Therefore, it is expected that in all directions, the points along the side area of the channel are the critical areas during deformation and are prone to failure (fracture onset).

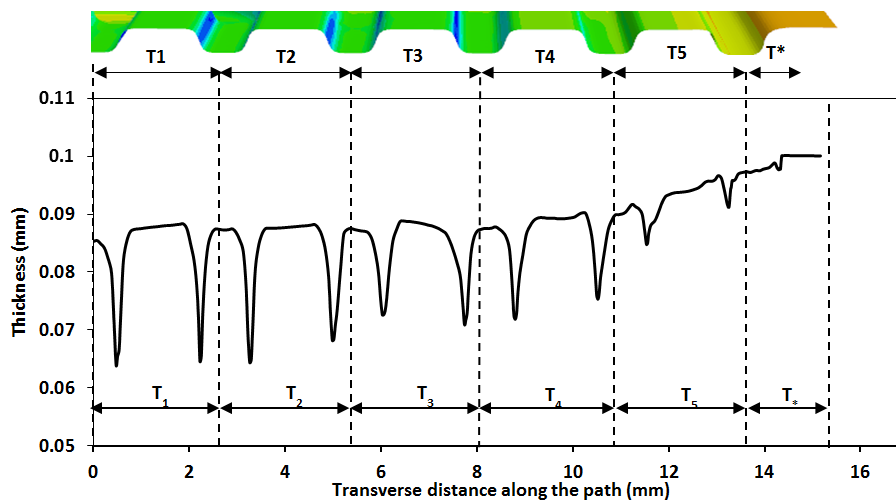


Fig. 11. Thickness distribution in the transverse direction.

To quantitatively evaluate the thickness reduction in different directions and to determine the critical direction, the thinning percentage based on the minimum thickness created in each area was calculated and is shown in Table 2. According to the results, the thin-

ning percentage increased in all directions by moving from the external channels to the internal channels. The thinning percentage in the outer channels in the diagonal, longitudinal, and transversal directions was 6.2, 3.9, and 2.3%, respectively.

Table 2. Maximum thinning percentage in various directions.

Direction	Thinning percentage in various areas					
	No. 1	No. 2	No. 3	No. 4	No. 5	No. *
Longitudinal	38.6	38.1	31.7	28.7	16.1	3.9
Diagonal	34.1	34.2	33.2	30.7	24.6	6.2
Transverse	36.0	35.6	29.0	27.8	8.8	2.3

In the middle channels in the above directions, the thinning percentages were 34.1%, 36%, and 38.6%, respectively. In the lateral regions, due to the strain caused by the corner radius (serpentine curvature), the amount of thinning in the diagonal direction (critical area in the lateral channels) was greater than in the other two directions.

On the other hand, a greater thinning percentage was observed as the sheet got closer to the middle channels. In the middle regions, the sheet elongation increased to fill the mold cavity. On the other hand, the longest channels were in the longitudinal direction. In other words, the highest level of contact with the mold (punch and die grooves) occurred in the channels along said path. Increased contact surface and its effect on the material flow (increasing friction and decreasing metal flow) is the main reason for the increase in thinning in this respect compared to the other two directions. Finally, it can be noted that the points located on the SAC are the most critical in forming MBPPs with a parallel-serpentine grooving pattern. Therefore, to produce high-quality MBPPs, the process should be designed in such a way that the deformation rate in this area does not exceed the permissible range.

Furthermore, the results indicate that multi-channel modeling alone cannot provide a detailed description of the metal flow in complex patterns. Considering the significant percentage of thickness reduction in MBPPs, and the impact on their performance under working conditions, the impact of lubricant application on the formation of MBPPs should be examined.

### **4.3. Effect of lubricant on thickness distribution**

According to the results presented earlier, signifi-

cant thinning percentages were observed in some areas of the formed MBPPs. To improve the thickness distribution process (reduction of thinning percentage difference and maximum thinning rate), lubricant-assisted MBPPs forming was also investigated. For this purpose, MBPPs were formed by the stamping process using a layer of polyethylene between the punch, the die, and the sheet. Then, the thickness distribution in the specimens was extracted from experimental tests using the method described in Section 2.2. The thickness distribution in the longitudinal direction of MBPPs formed under lubricated and non-lubricated conditions is shown in Fig. 12(a). The results show a significant improvement in the thickness distribution in the plates fabricated using a lubricant.

According to the results, the minimum thickness of MBPP micro-channels increased when using a lubricant (area B). On the other hand, the thickness in areas A, C, and E decreased when using lubricant compared to specimens produced in under-lubricated conditions. The use of a lubricant increases the sheet flow rate from A, C, and E to B and D by reducing the friction force. This ultimately results in a more uniform thickness distribution (lower thinning percentage difference) as well as a reduction in the maximum thinning.

Subsequently, the finite element modeling and definition of contact conditions were modified (with the help of experimental results) to provide a calibrated and validated model to predict the behavior of the sheet being formed using lubricants. A comparison between the experimental and simulation results (Fig. 12(b)) indicates that the Coulomb model of friction with a coefficient of friction of 0.1 provides a detailed description of the behavior of the contact surface and sheet flow. Hence, the results of process modeling with coefficients of friction of 0.1 were used for further studies.

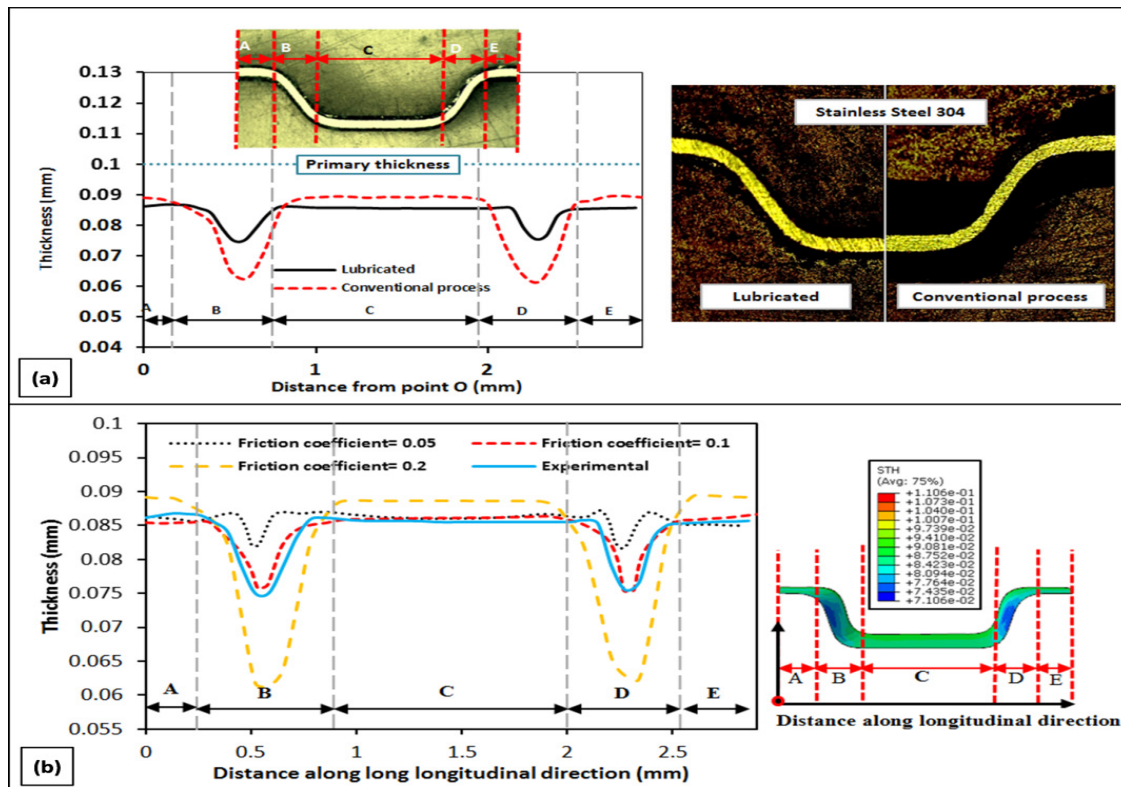


Fig. 12. Thickness distribution, (a) longitudinal direction of the sample fabricated under lubricated and non-lubricated conditions and (b) effect of friction coefficient.

#### 4.4. Thickness distribution process in different directions with lubricant

Changes in the thickness distribution in three directions, diagonal, longitudinal, and transversal, were investigated in the formed specimens when using a lubricant. For this purpose, the final thickness in the elements located in regions L1, D1, and T1 was extracted through finite element studies. This is shown in Fig. 13, along with the thickness distribution under non-lubricating conditions. According to the results, the use of lubricant improved the process of thickness distribution in all three directions (compared to the non-lubricated condition). The highest thinning percentages continued to occur in region A in the longitudinal direction (Fig. 13 (a)).

The maximum thinning percentage decreased from 38.6% under non-lubricated conditions to 24.7% in

specimens formed by using a lubricant. Furthermore, the maximum thinning percentage in the diagonal and transversal direction was calculated to be 28.4% and 23.5%, respectively, indicating a significant improvement under non-lubricated conditions (32.2% and 35.6% thinning in the diagonal and transversal directions). In contrast to non-lubricated conditions, the results showed the highest thinning percentage (among all directions) occurred under the lubricant-assisted forming condition in area D in the diagonal direction. In other words, the lubricant-assisted MBPP forming process causes the critical area to move from the SAC in the longitudinal direction to region D in the diagonal direction.

It is noteworthy to mention that there were no significant changes in the thickness distribution of areas close to the outer radius of the serpentine curvature located on the diagonal direction (equivalent to points *d*, *e*, and *f* in Fig. 8). Minimum thicknesses in these areas

occurred at points near the corner radius of the mold. In contrast to the SAC, the aforementioned areas were in contact with the die surface since the beginning of the process. Therefore, the use of lubricants did not significantly affect the thickness distribution in these areas in the diagonal direction (Fig. 13(b)). As a result, under lubricated conditions, the critical area moved from the SACs located in the longitudinal direction

to the areas close to the outer radius of the serpentine curvature (diagonal direction). The critical areas in terms of thinning percentage based on the obtained results under the lubricated and non-lubricated stamping process are shown in Fig. 14. These zones are susceptible to fracture during plastic deformation, and the material flow in these zones should be improved to increase the uniformity of the fabricated sample.

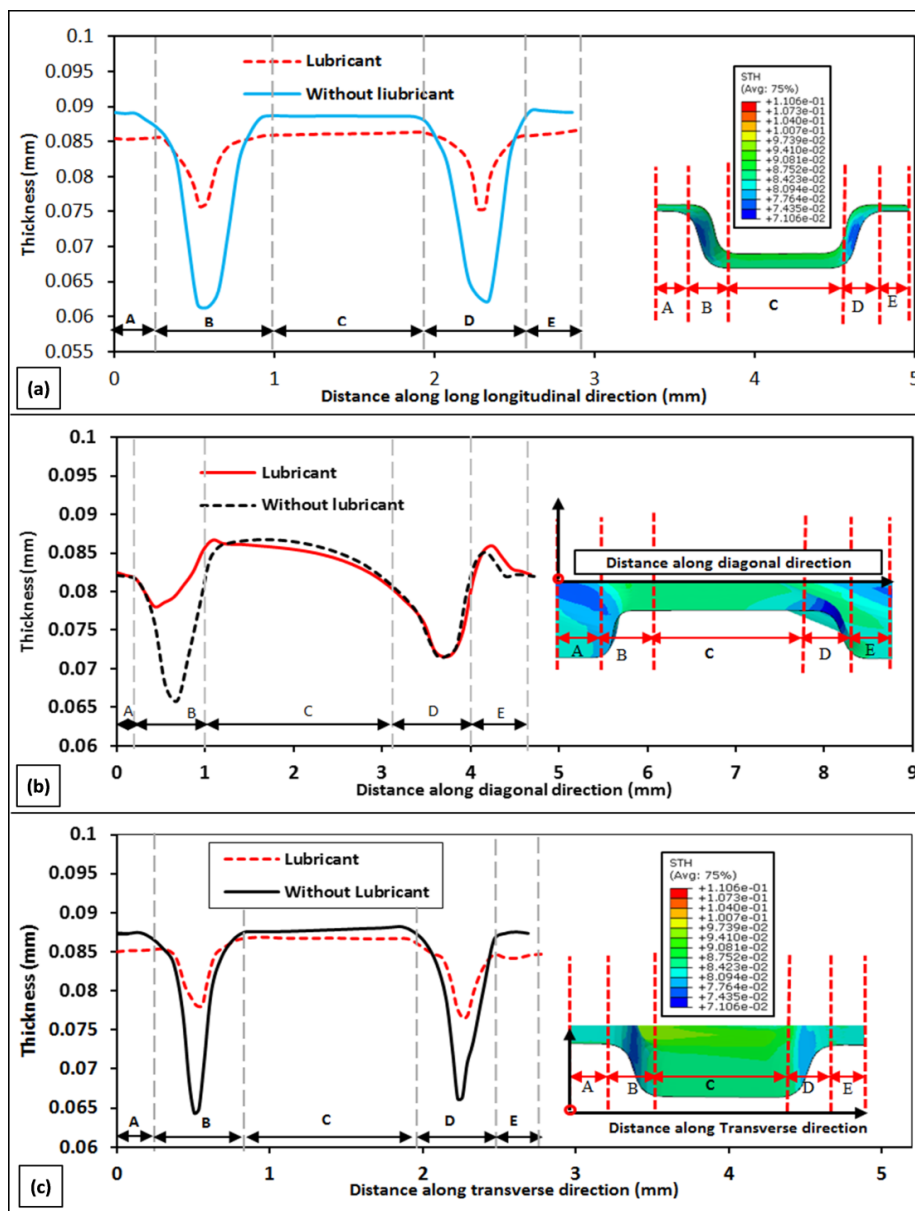


Fig. 13. Comparison of the thickness distribution under lubricated and non-lubricated conditions, (a) longitudinal direction, (b) diagonal direction, and (c) transverse direction.

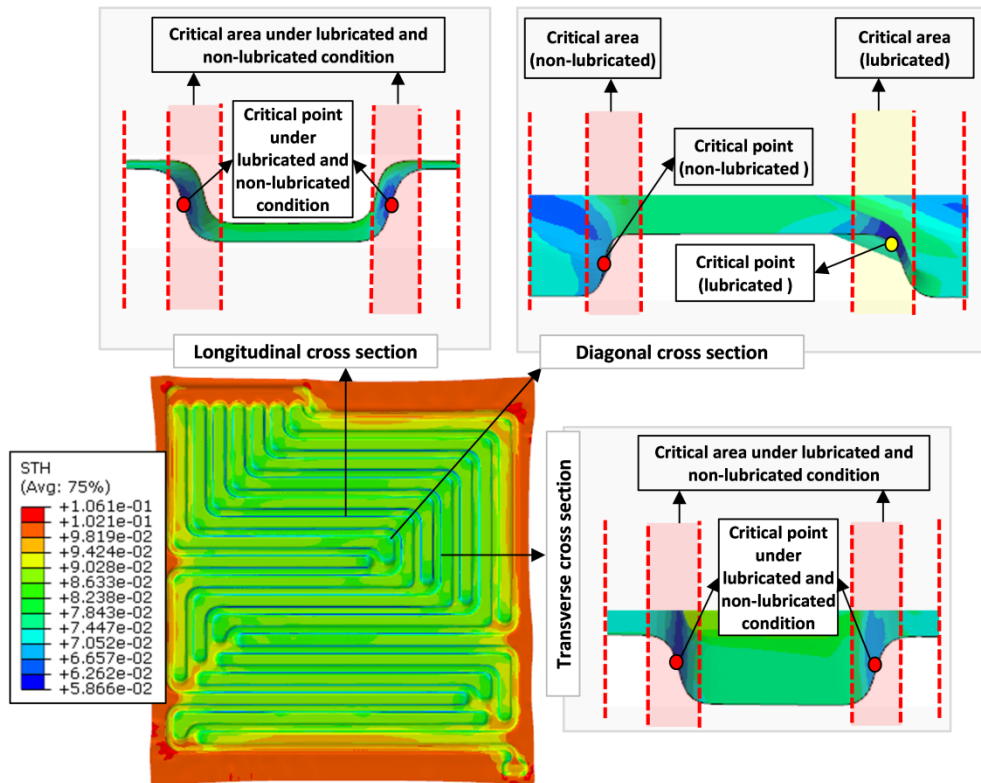


Fig. 14. Critical areas and points during stamping of MBPP.

## 5. Conclusion

In this study, the plastic deformation of an MBPP with a serpentine flow field was investigated during the stamping process. Experimental tests and FESs were used to fully understand the process of thickness distribution and strain path in different directions and regions of the bipolar plate. The results of the present study are summarized below:

- Increasing the forming force from 40 kN to 100 kN causes the filling rate to increase from 55.84% to 96.61%. The maximum thickness reduction in the critical area increases from 11.3% to 34.3% by increasing the force from 40 kN to 100 kN.
- The results indicate that the thickness of the specimen increases in the lateral area. The effect of sheet flow on the thickness distribution is visible in the three lateral channels and does not have a significant effect on the other channels.
- The highest thinning percentage occurs in the longitudinal direction for SS304 MBPPs. Thickness percentages in the diagonal, transversal, and longitudinal directions in plates formed to 0.65mm depth are 34.1%, 36%, and 38.6%, respectively.
- The use of a lubricant improves thickness distribution in SS304 BPPs. According to the results, the minimum thickness created when using the lubricant increases in the area of the SAC.
- According to the results, the maximum thinning percentage decreases in the longitudinal direction from 38.6% to 24.7% in the non-lubricated specimens and lubricant specimens, respectively. Furthermore, the maximum thinning percentage in the diagonal and transversal direction is calcu-

lated to be 28.4% and 23.5%, respectively. The thickness distribution in areas close to the outer radius of the serpentine curvature (in the diagonal direction) is approximately the same under lubricated and non-lubricated conditions.

## References

- [1] Chubbock S, Clague R. Comparative analysis of internal combustion engine and fuel cell range extender. *SAE International Journal of Alternative Powertrains*. 2016;5:175-82.
- [2] Barzegari MM, Rahgoshay SM, Mohammadpour L, Toghraie D. Performance prediction and analysis of a dead-end PEMFC stack using data-driven dynamic model. *Energy*. 2019;188:116049.
- [3] Alizadeh E, Ghadimi M, Barzegari M, Momenifar M, Saadat S. Development of contact pressure distribution of PEM fuel cell's MEA using novel clamping mechanism. *Energy*. 2017;131:92-7.
- [4] Barzegari MM, Dardel M, Alizadeh E, Ramiar A. Dynamic modeling and validation studies of dead-end cascade H<sub>2</sub>/O<sub>2</sub> PEM fuel cell stack with integrated humidifier and separator. *Applied energy*. 2016;177:298-308.
- [5] Silva R, Franchi D, Leone A, Pilloni L, Masci A, Pozio A. Surface conductivity and stability of metallic bipolar plate materials for polymer electrolyte fuel cells. *Electrochimica Acta*. 2006;51:3592-8.
- [6] Yan X, Hou M, Zhang H, Jing F, Ming P, Yi B. Performance of PEMFC stack using expanded graphite bipolar plates. *Journal of Power Sources*. 2006;160:252-7.
- [7] Minke C, Hickmann T, dos Santos AR, Kunz U, Turek T. Cost and performance prospects for composite bipolar plates in fuel cells and redox flow batteries. *Journal of Power Sources*. 2016;305:182-90.
- [8] Hung J-C, Chang D-H, Chuang Y. The fabrication of high-aspect-ratio micro-flow channels on metallic bipolar plates using die-sinking micro-electrical discharge machining. *Journal of Power Sources*. 2012;198:158-63.
- [9] Hung J-C, Yang T-C, Li K-c. Studies on the fabrication of metallic bipolar plates—Using micro electrical discharge machining milling. *Journal of Power Sources*. 2011;196:2070-4.
- [10] Lim S, Kim Y, Kang C. Fabrication of aluminum 1050 micro-channel proton exchange membrane fuel cell bipolar plate using rubber-pad-forming process. *The International Journal of Advanced Manufacturing Technology*. 2013;65:231-8.
- [11] Modanloo V, Talebi-Ghadikolaee H, Alimirzaloo V, Elyasi M. Fracture prediction in the stamping of titanium bipolar plate for PEM fuel cells. *International Journal of Hydrogen Energy*. 2021; 46: 5729-5739.
- [12] Lee S-J, Lai J-J, Huang C-H. Stainless steel bipolar plates. *Journal of Power Sources*. 2005;145:362-8.
- [13] Kahraman H, Orhan MF. Flow field bipolar plates in a proton exchange membrane fuel cell: Analysis & modeling. *Energy Conversion and Management*. 2017;133:363-84.
- [14] Karimi S, Fraser N, Roberts B, Foulkes FR. A review of metallic bipolar plates for proton exchange membrane fuel cells: materials and fabrication

- methods. *Advances in Materials Science and Engineering*. 2012;2012.
- [15] Yang G, Mo J, Kang Z, List III FA, Green Jr JB, Babu SS, et al. Additive manufactured bipolar plate for high-efficiency hydrogen production in proton exchange membrane electrolyzer cells. *international journal of hydrogen energy*. 2017;42:14734-40.
- [16] Mohammadtabar N, Bakhshi-Jooybari M, Hosseini-pour SJ, Gorji A. Study of effective parameters in hydroforming of fuel cell metallic bipolar plates with parallel serpentine flow field. *Modares Mechanical Engineering*. 2014;14.
- [17] Elyasi M, Talebi Ghadikolaee H, Hosseinzadeh M. Fabrication of metallic bipolar plates in PEM fuel cell using semi-stamp rubber forming process. *The International Journal of Advanced Manufacturing Technology*. 2017;92:765-76.
- [18] Talebi-Ghadikolaee H, Elyasi M, Mirnia MJ. Investigation of failure during rubber pad forming of metallic bipolar plates. *Thin-Walled Structures*. 2020;150:106671.
- [19] Abeyrathna B, Zhang P, Pereira MP, Wilkosz D, Weiss M. Micro-roll forming of stainless steel bipolar plates for fuel cells. *International Journal of Hydrogen Energy*. 2019;44:3861-75.
- [20] Barzegari MM, Khatir FA. Study of thickness distribution and dimensional accuracy of stamped metallic bipolar plates. *International Journal of Hydrogen Energy*. 2019;44:31360-71.
- [21] Hu Q, Zhang D, Fu H, Huang K. Investigation of stamping process of metallic bipolar plates in PEM fuel cell—Numerical simulation and experiments. *International Journal of Hydrogen Energy*. 2014;39:13770-6.
- [22] Bong HJ, Lee J, Kim J-H, Barlat F, Lee M-G. Two-stage forming approach for manufacturing ferritic stainless steel bipolar plates in PEM fuel cell: Experiments and numerical simulations. *International Journal of Hydrogen Energy*. 2017;42:6965-77.
- [23] Choi S-W, Park SH, Jeong H-S, Cho J, Park S, Ha MY. Improvement of formability for fabricating thin continuously corrugated structures in sheet metal forming process. *Journal of mechanical science and technology*. 2012;26:2397-403.
- [24] Jin CK, Koo JY, Kang CG. Fabrication of stainless steel bipolar plates for fuel cells using dynamic loads for the stamping process and performance evaluation of a single cell. *International Journal of Hydrogen Energy*. 2014;39:21461-9.
- [25] Neto DM, Oliveira MC, Alves JL, Menezes LF. Numerical study on the formability of metallic bipolar plates for proton exchange membrane (PEM) fuel cells. *Metals*. 2019; 9: 810.
- [26] Ahmadi Khatir F, Barzegari MM, Talebi-Ghadikolaee H, Seddighi S. Integration of design of experiment and finite element method for the study of geometrical parameters in metallic bipolar plates for PEMFCs. *International Journal of Hydrogen Energy*. 2021; 46: 39469-39482.